HHS Public Access

Author manuscript

Structure. Author manuscript; available in PMC 2019 August 07.

Published in final edited form as:

Structure. 2018 August 07; 26(8): 1137–1143.e3. doi:10.1016/j.str.2018.05.008.

Structural basis for MARK1 kinase autoinhibition by its KA1 domain

Ryan P. Emptage[1,*], **Mark A. Lemmon**[2], **Kathryn M. Ferguson**[2], and **Ronen Marmorstein**[1,3,*]

[1]Department of Biochemistry and Biophysics and the Abramson Family Cancer Research Institute, Perelman School of Medicine, University of Pennsylvania, Philadelphia, Pennsylvania 19104, USA

[2]Department of Pharmacology and Cancer Biology Institute, Yale University School of Medicine, New Haven, CT 06520, USA

[3]Department of Chemistry, University of Pennsylvania. Philadelphia, PA 19104, USA

SUMMARY

The kinase associated-1 (KA1) domain is found at the C-terminus of multiple Ser/Thr protein kinases from yeast to humans, and has been assigned autoinhibitory, membrane-binding, and substrate-targeting roles. Here, we report the crystal structure of the MARK1 kinase/UBA domain bound to its autoinhibitory KA1 domain, revealing an unexpected interface at the αD-helix and contacts with both the N- and C-lobes of the kinase domain. We confirm the binding interface location in kinetic studies of variants mutated on the kinase domain surface. Together with other MARK kinase structures, the data implicates that the KA1 domain blocks peptide substrate binding. The structure highlights the kinase-specific autoinhibitory binding modes of different KA1 domains, and provides potential new avenues by which to intervene therapeutically in Alzheimer's disease and cancers in which MARK1 or related kinases are implicated.

Graphical abstract

*Correspondence: emptage@upenn.edu, marmor@upenn.edu.

AUTHOR CONTRIBUTIONS

Conceptualization, R.P.E.; Investigation, R.P.E.; Writing – Original Draft R.P.E.; Writing – Review & Editing, R.P.E., M.A.L., K.M.F., and R.M.; Supervision M.A.L., K.M.F., and R.M.; Funding Acquisition, R.P.E. and R.M.

DECLARATION OF INTERESTS

The authors declare no competing interests.

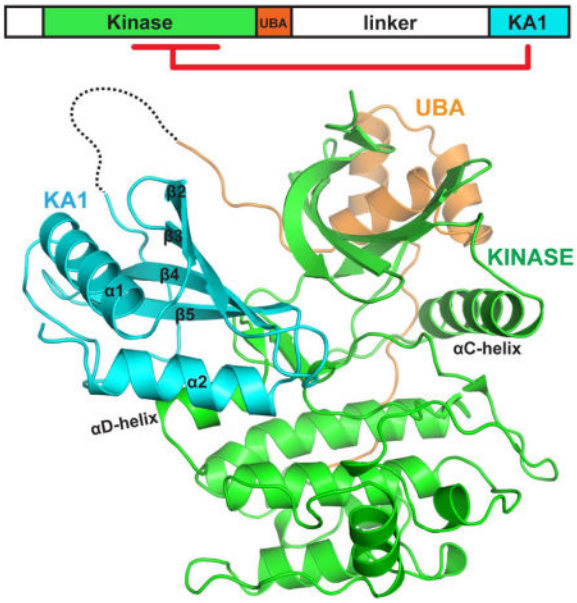

Keywords

MARK1; Serine/threonine protein kinase; autoinhibition; C-terminal domain; inhibitory mechanism; structural biology; activation segment; Tau protein; αD-helix

INTRODUCTION

Despite a high degree of conservation in their kinase catalytic domain, the ~500 members of the human kinome family vary widely in their mechanisms of regulation (Manning et al., 2002; Pawson and Kofler, 2009). A plethora of domain types, including SH2, SH3, C1, C2, and PH domains, function as spatiotemporal allosteric regulators of kinase activity. These regulatory domains may bind intermolecularly to modulate kinase activity in *trans*, or intramolecularly within the same polypeptide chain. Although well described for several kinase subfamilies, intramolecular allosteric regulation is not well understood for an important subgroup of Ca^{2+}/calmodulin-dependent protein kinases (CAMK), known as CAMK-like or CAMKL kinases. This group includes the MARK/PAR1 kinases (for MAP/Microtubule affinity-regulating kinases), which have been implicated in a significant subset of cancers (Goodwin et al., 2014; Monteverde et al., 2015). MARKs and other CAMKL kinases have a characteristic domain architecture consisting of the catalytic domain and an ubiquitin-associated (UBA) domain – connected via an unstructured linker region to a C-terminal kinase associated-1 (KA1) domain (Fig. 1A) (Marx et al., 2010). The KA1 domain is relatively small (~14 kDa), and comprises a 4-stranded β-sheet flanked by two α-helices. With strong structural conservation despite low sequence identity, KA1 domains are found in CAMKL family members as far back as yeast (Emptage et al., 2017b; Moravcevic et al., 2010; Tochio et al., 2006). One noted feature of the KA1 domain is its affinity for anionic membranes (Moravcevic et al., 2010), but how this feature relates to the proposed regulatory functions of the module has remained unclear until recently (Emptage et al., 2017a; Emptage et al., 2017b; Wu et al., 2015).

Prompted by reports that KA1 domains of related protein kinases may regulate catalytic domain activity (Marx et al., 2010; Wu et al., 2015), we showed previously that the KA1 domain of human MARK1 is an intramolecular autoinhibitory domain that interacts directly with the catalytic domain (Emptage et al., 2017a). The observation that binding of the KA1 domain to anionic vesicles was diminished in the presence of the catalytic domain led us to propose that binding of anionic phospholipid membranes to the KA1 domain reverses MARK1 autoinhibition, which we demonstrated *in vitro* by stimulating autoinhibited MARK1 activity upon exposure to anionic vesicles. We were able to infer which face of the KA1 domain mediates autoinhibition using mutagenesis (Emptage et al., 2017a), but the interaction has not been characterized structurally. Here, we describe the crystal structure of the MARK1 catalytic domain bound to the KA1 domain. The structure demonstrates a direct interaction and reveals details of the autoinhibitory interface, which engages both the N- and C-lobes of the kinase domain and is likely to compete with peptide substrate for binding to the kinase (Nesic et al., 2010). The structure advances molecular understanding of protein kinase regulation by KA1 domains. Given the implication of CAMKL kinases in multiple diseases, including the importance of Tau phosphorylation by MARK1 in Alzheimer's disease (Chin et al., 2000), visualizing this mode of kinase regulation may illuminate new avenues for developing structure-based approaches to modulating MARK/PAR family kinases therapeutically.

RESULTS

Crystal structure of autoinhibited MARK1

We previously characterized a stable, KA1-autoinhibited form of MARK1 ('mini' MARK1) from which both the 299 amino acid linker and the 45 amino acid N-terminal unstructured region have been deleted (Fig. 1A). We demonstrated that 'mini' MARK1 harboring a kinase activation loop phosphomimetic mutation (T215E) is autoinhibited by the KA1 domain and can be activated by anionic membranes (Emptage et al., 2017a) – likely mimicking regulation of intact MARK1 *in vivo*. Efforts to crystallize this particular protein construct were unsuccessful, so we attempted to crystallize the KA1-mutated constructs of our previous study that retained autoinhibition, which we had generated to identify the autoinhibitory interface through mutagenesis. Crystals diffracting to 2.5 Å resolution were obtained using a construct harboring two additional mutations in the KA1 domain (K761S/R764S) that we showed do not perturb autoinhibition (Emptage et al., 2017a) or phospholipid binding (Moravcevic et al., 2010). Initial phases were generated by molecular replacement using structures of the MARK1 WT kinase/UBA domain (PDB: 2HAK) and KA1 domain (PDB: 3OSE) as search models, and the initial model was refined to an R_{work}/R_{free} of 20.2/25.2 (Table 1). The final model contains two polypeptides in the asymmetric unit (Fig. S1A). Chain A (Fig. 1B) contains MARK1 residues 53-377 (kinase/UBA domains) and 696-795 (KA1 domain). The 18 residues that link these two parts of 'mini' MARK1, which are missing due to lack of electron density, span 18.7 Å (Fig. S1B). They would need to span >65 Å for the alternative chain assignment (in which the KA1 domains of chain A and B are swapped), which is an unlikely (if not impossible) distance for 18 residues to extend. Chain B contains kinase/UBA residues 53-373 and KA1 domain residues 695-795 in an identical conformation to Chain A (Fig. S1A).

Two possible kinase/KA1 domain interfaces are observed in the crystal lattice (Fig. S1A). One occurs between domains within the same polypeptide chain, between Kinase^{A} (green) and KA1^{A} (cyan), as shown in Fig. 1B. The other occurs between chains and contributes to dimerization in the crystal: Kinase^{A} (green) and KA1^{B} (salmon) in Fig. S1A. In the intramolecular Kinase^{A}/KA1^{A} interaction, the KA1 domain packs against helix αD of the kinase domain within the same chain to bury 779.2 Å^2 of surface area (Fig. 1B). By contrast, in the intermolecular interaction the KA1 domain abuts the αC-helix of a symmetry related kinase/UBA domain and buries 701.3 Å^2 of surface (Fig. S1A -Kinase^{A}/KA1^{B}). Although the αC helix is frequently a site of regulatory interactions in kinases, both structural and experimental considerations lead us to propose that the intermolecular KA1 domain interaction of the MARK1 αC-helix (Fig. S1C) reflects only crystal packing interactions, whereas the interface at the helix αD (Fig. 1C) represents the biologically relevant interface. This conclusion is supported by our previous observations that an analogous construct (albeit without the K761S/R764S mutation) remains monomeric in solution at 140 M (Emptage et al., 2017a). In addition, in the intermolecular helix αC interface, the side chain of the serine that replaces the native R764 (in R764S) contacts the αC helix directly, providing a structural rationalization as to why mutation at that position aided crystallization. Indeed, the native arginine at that position would clash with helix αC (Fig. S1D) – and this interface would not be made with the wild-type KA1 domain

The intramolecular helix αD interface with the KA1 domain (Fig. 1B,C) engages strand β4, strand β5, and helix α2 of the KA1 domain, including the side chains of residues E756, K773, R774, and K783, of which all but E756 were implicated in kinase inhibition in our previous studies (Emptage et al., 2017a) – but do not participate in the intermolecular kinase/KA1 interaction (Fig. S1C). Side chains of R698, R701, K707, and K788, also implicated in kinase inhibition previously (Emptage et al., 2017a), reside in the vicinity of the binding interface though do not contact the kinase domain directly in our structure (Fig. 1C). Residues previously implicated in membrane association, especially K773 and R774 (Moravcevic et al., 2010), populate this interface (Fig. 1B *right panel*, Fig. 1C), providing a structural rationale for release of autoinhibition upon membrane binding. The kinase helix αD residues V149, A150, and H151 all participate in interactions with the KA1 domain, with direct packing between the side-chains of V149 in the kinase and F782 in the KA1 domain (Fig. 1C). The side-chain of D146 also forms a water-mediated interaction with the backbone amide of R774 in strand β5, and the E143 side chain forms a predicted salt bridge with the KA1 domain R774 side chain (Fig. 1C, S1E). A backbone-backbone amide to carbonyl hydrogen bond is formed between the K68 backbone amide in strand β1 of the kinase domain and the carbonyl of I775 in strand β5 in the KA1 domain, and the K64 side-chain in strand β1 of the kinase forms a predicted salt bridge with the E756 side-chain in strand β4 of the KA1 domain. These and other interactions yield an intimate interface.

Kinetic validation of the kinase domain-KA1 interface

To investigate the biological relevance of the intramolecular KA1/kinase interface detailed in Fig. 1C, we assessed the ability of differently mutated kinase/UBA domain proteins at 5 μM to be *trans*-inhibited by separately purified KA1 domain at 200 μM, a concentration responsive to changes in inhibitory activity (Fig. 1D) (Emptage et al., 2017a). Mutating

residues in the intermolecular (αC helix) interface, including K93, L101, Q102, F105, and E127 had no significant effect, despite the engagement of these side-chains in the KA1/kinase interface shown in Fig. S1C. KA1 domain-mediated inhibition was also unaffected by mutating UBA domain residues N355 and K357, which contribute to the intermolecular KA1 domain interactions of the crystal structure. Mutating W704/M706 in the KA1 domain, which contact the kinase domain αC-helix in the intermolecular interaction also failed to impair *trans*-inhibition capability (Fig. 1D, last bar), arguing that these residues, which dominate the intermolecular KA1/kinase interaction (Fig. S1C), do not play a significant role in autoinhibition. By contrast, mutating kinase domain residues engaged in the αD-centered intramolecular interface described above (E143, D146, V149, A150, and H151) prevented the wild-type KA1 domain from *trans*-inhibiting the MARK1 kinase domain (Fig. 1D).

Fig. S2 shows the crystal structure of autoinhibited kinase/UBA chain A with both $KA1^{A}$ and $KA1^{B}$ displayed. Onto this structure, we mapped locations of kinase/UBA (Fig. S2A) and KA1 (Fig. S2B) mutations – from this and our previous study (Emptage et al., 2017a). Mutations that abrogate kinase inhibition by the KA1 domain are represented as black spheres, and those that do not affect inhibition are grey. This analysis reveals that mutations in the intramolecular $KA1^{A}$/$kinase^{A}$ interface, in and around the αD-helix of the kinase, block inhibition, whereas those in the intermolecular $KA1^{B}$/$kinase^{A}$ interface do not – and are grey – supporting our assignment of the interface at the kinase αD-helix as the biologically relevant autoinhibitory (intramolecular) KA1 domain-kinase/UBA interaction.

Structural insights into the inhibitory mechanism of the KA1 domain

Because the structure reported here contains the phosphomimetic T215E activation segment mutation, it captures the first snapshot of MARK1 in the active-like conformation. This conformation includes closure of the N-lobe/UBA module upon the active site and movement of helix αC-helix from the inactive 'αC-out' to the active 'αC-in' position when compared with the previously determined structure of the MARK1 kinase/UBA domain (Fig. 2A) (Marx et al., 2006). Closure is concurrent with a resolved, outstretched activation segment in which T215E and C217 of this loop make hydrogen bonds with residues R106 and K103 of the αC-helix, respectively, and the DFG and HRD motifs are flipped into their catalytically-competent conformations (Fig. 2A, inset). Our previous data argue that the KA1 domain can inhibit both wild-type and T215E MARK1 kinase/UBA domains, indicating that interactions of the KA1 domain with the N-lobe that occur in conjunction with the closed conformation may not be necessary for inhibitory activity (Emptage et al., 2017a). Alternatively, the KA1 domain may induce a closed active-like conformation even in the absence of the T215E phosphomimetic mutation, or phosphorylation of this residue *in vivo*.

Intriguingly, a related structure of the wild-type MARK2 kinase/UBA domain in complex with a peptide inhibitor from the CagA virulence factor of *Helicobacter pylori* (Nesic et al., 2010) reveals that the CagA inhibitor induces a closed αC-in active-like conformation of the catalytic domain, even though the MARK2 kinase construct does not harbor a phosphomimetic mutation in the activation loop (Fig. 2B). Thus, both the *H. pylori*

inhibitory peptide and the KA1 domain appear to inhibit MARKs in an active-like conformation with αC in and with the activation segment extended outward. Additionally, the KA1 domain binding site on MARK1 overlaps the binding site for the peptide inhibitor on MARK2 – which likely mirrors the peptide substrate binding site of MARK kinases. Based on the overlay shown in Fig. 2B, the KA1 domain and peptide substrate would not be able to bind MARK1 simultaneously. The acidic cleft located below the αD-helix on the kinase domain has been previously noted as an important anchoring point for basic residues N-terminal to the phosphorylation site for other protein kinases such as PKA and Akt (de Oliveira et al., 2016; Miller and Turk, 2018), and interference at this site from the MARK1 KA1 domain may underlie its autoinhibitory activity.

Despite a high degree of structural homology, we have reported that modes by which KA1 domains inhibit kinase activity are highly specific to their conjugate kinase (Emptage et al., 2017a; Emptage et al., 2017b). This observation is further reinforced by the only previously determined crystal structure of a KA1 domain bound to a protein kinase catalytic domain, that of murine SAD-A, a human BRSK2 ortholog (Fig. 2C) (Wu et al., 2015). In the SAD-A structure, both the UBA and KA1 domains are positioned differently on the sides of the N-lobe compared to our MARK1 structure, and the main interactions with the catalytic domain occur through hydrophobic side chains in the autoinhibitory sequence (AIS) of SAD-A. Kinetic studies reveal this AIS to be sufficient for inhibition of the kinase/UBA domain of SAD-A (Wu et al., 2015). By contrast, the MARK1 KA1 domain lacks the AIS (Wu et al., 2015) and clearly relies on other regions of the KA1 domain to assert its inhibitory activity (Fig. 2C). Residues W704/M706 of the crystallographic interface that make analogous interactions with the N-lobe when compared to the SAD-A AIS (Fig. S1C) are not required for inhibitory activity in the case of MARK1 (Fig. 1D).

DISCUSSION

The crystal structure reported herein represents an activation segment-out (phosphorylation mimic state), and αC-in form of MARK1 that is autoinhibited by the bound KA1 domain. The structure reveals that the KA1 domain is able to inhibit the kinase in its active conformation, but given the ability of αD-helix mutants of otherwise WT catalytic domain to prevent inhibition by the KA1 domain (Fig. 1D), this binding site is also utilized in the absence of activating phosphorylation at T215. Based on our previous data showing that autoinhibited MARK1 is activated by KA1 domain-mediated localization to anionic phospholipid vesicles (Emptage et al., 2017a), we postulate that relief of autoinhibition represents an additional step in MARK1 activation, occurring after activation segment phosphorylation by kinases such as LKB1 (Fig. 3) (Lizcano et al., 2004). In this model, an inactive/autoinhibited form of MARK1 is phosphorylated by cytosolic kinases, which could increase activity ~10-fold (even the presence of the KA1 domain) based on our experiments with the phosphomimetic T215E mutation (Emptage et al., 2017a). Subsequent localization to anionic membranes would then disengage the *cis*-interacting KA1 domain from the autophosphorylated kinase, and cause an additional ~10-fold increase in activity (Emptage et al., 2017a). Thus, the activity of MARK1 appears to be modulated by several orders of magnitude based on phosphorylation state and cellular localization (Fig. 3). An analogous second step of activation may be driven by MARK1 binding to peptide ligands of the KA1

domain, such as GAB1 (Yang et al., 2012). Given that the KA1 domain inhibits both T215E and WT kinase domain (Emptage et al., 2017a) and recent findings that LKB1 is also activated by anionic phospholipids (Dogliotti et al., 2017), phosphorylation at T215 may not necessarily precede relief of autoinhibition, and the order of MARK1 activation may depend on cellular context.

A key common feature of KA1 domains is the presence of clusters of basic residues on their surface (Emptage et al., 2017b; Moravcevic et al., 2010). Charge complementarities are likely to play a role in the autoinhibitory interactions of a KA1 domain with its cognate kinase domain, as illustrated for MARK1 in Fig. 4 (upper), but our structural and mutational data show that the interactions also employ highly sequence-specific elements – so that each kinase is inhibited by only its cognate KA1 domain (Emptage et al., 2017a; Emptage et al., 2017b). Given the divergent inhibitory mechanism of the SAD-A KA1 domain mentioned above (Fig. 2C), there may be multiple additional modes of kinase inhibition by KA1 domains yet to be uncovered for other kinases (Wu et al., 2015). The higher affinity of the separately purified Chk1 KA1 domain for its cognate kinase compared to MARK1 kinase may arise in part from the higher prevalence of acidic residues on the Chk1 kinase surface (Fig. 4, *lower panel*) (Emptage et al., 2017a; Emptage et al., 2017b). This observation, combined with the fact that Chk1 is activated through phosphorylation at the linker region and not the activation segment (Smits and Gillespie, 2015), suggests that KA1 domain-mediated Chk1 autoinhibition, and relief of autoinhibition through phosphorylation, may employ an alternative mechanism than seen with MARK1.

Differences among CAMKL and related kinases at the sequence level highlight which kinases may employ a similar autoinhibitory mechanism to MARK1. Within the KA1 domain, the kinase-interacting residues E756, R771, K773, R774, F782, and K783 are highly conserved among the MARKs, though the RXKR motif on strand β5 is slightly less so in the yeast KA1-containing kinases such as Kcc4 and Hsl1 (Moravcevic et al., 2010). Although the Chk1 KA1 does not have a residue analogous to E756 on strand β4, it does have multiple basic residues on strand β5, and an FK motif on helix α2 analogous to residues 782-783 of MARK1 (Emptage et al., 2017b). SAD-A has basic residues at α2, but lacks conservation of the other residues involved in the MARK1 autoinhibitory interface, possibly explaining the divergence of its inhibitory mechanism (Wu et al., 2015). With regards to kinase domain residues involved in the MARK1 autoinhibitory interaction, K64 of the N-lobe is conserved among numerous protein kinases (Fig. S3). Amongst the acidic residues of the αD-helix, E143 is conserved in all MARKs and even protein kinase A (PKA). However, PKA does not contain an analogous residue to D146, nor the VAH motif at positions 149-151 which is common to the MARKs. Chk1 lacks an analog for K64 or the VAH motif, again suggesting it may be autoinhibited by a different binding modality (Fig. S3).

Given the apparent specificity of each kinase-KA1 conjugate pair, and the uniqueness of KA1-mediated autoinhibition when compared to regulation of the rest of the human kinome, opportunity exists to target these specific interactions with small molecule probes. The vast majority of FDA-approved small-molecule protein kinase therapeutics are designed to bind a conserved ATP-binding pocket. While high affinity has been achieved by tailoring these

inhibitors for the kinase in question, off-target interactions with other kinases can derail the clinical efficacy of these compounds, especially in the case of the CAMKL family member Chk1 (Manic et al., 2015). The work described here could lay the foundation for strategies by which inhibitors may target the specific regulatory mechanisms of KA1 domain-containing kinases in order to exploit the highly specific nature of these interactions for higher drug selectivity in clinical settings.

STAR METHODS

Key Resources Table

REAGENT or RESOURCE	SOURCE	IDENTIFIER
Bacterial and Virus Strains		
Overexpress C41(DE3)	Sigma Aldrich	Cat#CMC0017
Chemicals, Peptides, and Recombinant Proteins		
Recombinant human MARK1 45-795, Δ382-681, T215E/ K761S/R764S, N-terminal hexahistidine (Crystal construct)	(Emptage et al., 2017a)	N/A
Recombinant human MARK1 45-371, TEV-cleavable N-terminal hexahistidine (kinase/ UBAdomain)	(Emptage et al., 2017a)	N/A
Recombinant human MARK1 683-795, N-terminal hexahistidine (KA1 domain)	(Moravcevic et al, 2010)	N/A
Tau-derived MARK1 substrate peptide	Genscript	Cat#RP20244
Recombinant TEV protease	pRK793	N/A
Deposited Data		
Crystal structure of autoinhibited MARK1	This study	6C9D
Recombinant DNA		
pET21a Recombinant human MARK1 45-795, Δ382-681, T215E/K761S/R764S, N-terminal hexahistidine (Crystal construct)	(Emptage et al., 2015a)	N/A
pET21a Recombinant human MARK1 45-371, TEV-cleavable N-terminal hexahistidine (kinase/UBA domain)	(Emptage et al., 2015a)	N/A
pET21a Recombinant human MARK1 683-795, N-terminal hexahistidine (KA1 domain)	(Moravcevic et al, 2010)	N/A
pRK793 (TEV protease)	Addgene	Plasmid#8827
Software and Algorithms		
HKL2000	(Otwinowski and Minor, 1997)	www.hkl-xray.com
Coot	(Emsley et al., 2010)	www2.mrc-lmb.cam.ac.uk/personal/pemsley/coot
PHENIX	(Adams et al., 2010)	www.phenix-online.org/documentation/index.html
MOLPROBITY	(Chen et al., 2010)	http://molprobity.biochem.duke.edu

REAGENT or RESOURCE	SOURCE	IDENTIFIER
PyMol	Schrödinger	www.pymol.org
APBS	(Baker et al., 2001)	www.poissonboltzmann.org/apbs
GraphPad Prism 5	GraphPad Software, Inc.	www.graphpad.com/scientific-software/prism/
PISA	(Krissinel and Henrick, 2007)	www.ebi.ac.uk/pdbe/pisa/
ESPript	(Robert et al., 2014)	http://espript.ibcp.fr
Other		
HisPur Ni-NTA Resin	Thermo Scientific	Cat#88223
HiTrap SP HP	GE Healthcare	Cat#17115101
Superdex 75 10/300 GL	GE Healthcare	Cat#17517104

Contact for Reagent and Resource Sharing—Further information and requests for resources and reagents should be directed to and will be fulfilled by the Lead Contact, Ronen Marmorstein (marmor@upenn.edu).

Method Details

Cloning, Expression, and Purification of MARK1 Constructs—The crystal construct was previously reported (Emptage et al., 2017a), containing MARK1 residues 45-795 (from which residues 382-681 were deleted), with an N-terminal hexahistidine tag appended, and inclusion of T215E, K761S, and R764S point mutations. Point mutations of a previously reported kinase/UBA MARK1 construct (residues 45-371 with an N-terminal tobacco etch virus (TEV) cleavable hexahistidine tag) (Emptage et al., 2017a) and the W704A/M706A mutant of the MARK1 KA1 domain construct (residues 683-795 with N-terminal hexahistidine tag) (Moravcevic et al., 2010) were generated using ‘round the horn’ site-directed mutagenesis (Hemsley et al., 1989) in a pET21a (EMD Millipore) expression vector. All expression constructs were transformed into Overexpress C41(DE3) *E. coli* (Sigma Aldrich). 6 mL LB overnights were used to inoculate 1 L cultures, grown at 37°C until the OD_{600} reached 0.6, and induced with 1 mM isopropyl-β-D-thiogalactoside 16 hr at 20°C.

All purification steps were performed at 4°C. PBS-w ashed cell pellets containing the MARK1 crystal construct were resuspended in a lysis buffer containing 25 mM Tris pH 8, 0.15 M NaCl, 5% (v/v) glycerol, 1 mM phenylmethylsulfonyl fluoride, and 5 mM β-mercaptoethanol (βME), and sonicated. Clarified cell lysates were subjected to affinity chromatography over Ni-NTA agarose (Thermo Scientific), with a wash step using 0.05 M imidazole and elution with 0.3 M imidazole, both in lysis buffer. Elution fractions were dialyzed against 25 mM MES pH 6, 0.1 mM NaCl, 5% (v/v) glycerol, and 5 mM βME, and were loaded onto a HiTrap SP HP column (GE Healthcare) from which protein was eluted using a gradient to 1 M NaCl in this same buffer. Ion exchange elution fractions were subjected to size exclusion chromatography (SEC) over a Superdex 75 column (GE Healthcare) with a running buffer of 20 mM Hepes pH 7.5, 150 mM NaCl, and 1 mM tris(2-carboxyethyl)phosphine. Concentrated peak fractions were stored at 4°C.

Kinase/UBA WT and point mutated constructs used in assays were purified as above with the following modifications. Following affinity chromatography, the N-terminal hexahistidine tag was removed with TEV protease during a dialysis step in 25 mM Tris pH 8, 0.3 M NaCl, 5% (v/v) glycerol, and 5 mM βME, and a reverse Ni-NTA affinity chromatography step was employed. The flow-through was collected and subjected to SEC as above. Concentrated peak fractions were stored frozen at −80°C.

KA1 constructs (WT and W704A/M706A) were purified from inclusion bodies as reported for the Chk1 KA1 domain (Emptage et al., 2017b). The insoluble pellets obtained after clarifying sonicated lysates were homogenized and briefly sonicated in 6 M guanidine HCl, 25 mM Tris pH 8, 0.25 M NaCl, 5 mM βME, and 10 mM imidazole. Affinity chromatography over Ni-NTA agarose included a 0.025 M imidazole wash step and 0.3 M imidazole elution step, both in homogenization buffer. Elution fractions were dialyzed against 25 mM Tris pH 8, 0.15 M NaCl, 10% (v/v) glycerol, and 5 mM βME, and subjected to SEC as above. Concentrated peak fractions were stored frozen at −80°C.

Crystallization, Data Collection, and Structure Determination—Protein expressing using the crystallization construct was concentrated to 15 mg/ml and incubated in hanging drop format in a 1:1 ratio with reservoir solution containing 6-8% (w/v) PEG 8000 and 0.2-0.3 M imidazole pH 8-8.5. Crystals appeared after one week, were cryo-protected in a solution of 25% (w/v) PEG 3350 and 5% (v/v) glycerol, and flash frozen in liquid nitrogen. Diffraction data were collected at the NECAT 24-ID-C beamline at the Advanced Photon Source, and reduced and scaled using HKL-2000 (Otwinowski and Minor, 1997). Initial phases were generated by iterative molecular replacement using the PHASER module in the PHENIX software suite (Adams et al., 2010), using multiple search ensembles, which were comprised of the MARK1 N-lobe, C-lobe, UBA (from PDB: 2HAK), and KA1 domain (PDB: 3OSE). The model was manually rebuild in COOT (Emsley et al., 2010) between rounds of iterative maximum-likelihood refinement in PHENIX, and the resulting model was validated with MOLPROBITY (Chen et al., 2010). Figures, including electrostatic surfaces, were generating using Pymol (Schrödinger).

Kinase Assay—The MARK1 kinase/UBA and point mutated constructs were assayed as previously reported (Emptage et al., 2017a). Assay conditions included 25 mM Hepes pH 7.5, 1 mM DTT, 5 mM $MgCl_2$, 0.1 mM ATP, and 0.1 mM Tau-derived peptide substrate, NVKSKIGSTENLK (Genscript). Enzyme in SEC buffer was diluted 5-fold into the assay to begin the reaction. Product formation was monitored with trace amounts of γ-^{32}P labeled ATP (~20 μCi per experiment) being transferred to peptide trapped onto phosphocellulose paper and reaction quenched with a 0.5% (w/v) phosphate solution. Following three phosphate washes and one with acetone, radioactivity of the phosphocellulose squares was quantified by scintillation counting. Reaction velocity was calculated as peptide substrate phosphorylated per enzyme molecule per minute with appropriate background correction.

Quantification and Statistical Analysis—Statistics generated from X-ray crystallography data processing, refinement, and structure validation are displayed in Table 1. Elevated B-factors are likely a result of radiation damage due to lowered attenuation of the synchrotron source, necessary to achieve a complete dataset at 2.5 Å. Buried surface

areas and free energy of solvation values were calculated using the PISA server (Krissinel and Henrick, 2007). Electrostatic surface potential was generated using the Adaptive Poisson-Boltzmann Solver (Baker et al., 2001).

Data and Software Availability—The coordinate and structure factor files for the crystal construct are deposited in the Protein Data Bank under accession code 6C9D.

Supplementary Material

Refer to Web version on PubMed Central for supplementary material.

Acknowledgments

This work was funded in part by NIH postdoctoral fellowships F32-GM115098 and T32-DK007780 (R.P.E.), and NIH grant P01-CA114046 (R.M.). This work is based upon research conducted at the Northeastern Collaborative Access Team beamlines, which are funded by the National Institute of General Medical Sciences from the National Institutes of Health (P41 GM103403). The Pilatus 6M detector on 24-ID-C beam line is funded by a NIH-ORIP HEI grant (S10 RR029205). This research used resources of the Advanced Photon Source, a U.S. Department of Energy (DOE) Office of Science User Facility operated for the DOE Office of Science by Argonne National Laboratory under Contract No. DE-AC02-06CH11357. We would like to thank the beamline staff for their assistance.

References

Adams PD, Afonine PV, Bunkoczi G, Chen VB, Davis IW, Echols N, Headd JJ, Hung LW, Kapral GJ, Grosse-Kunstleve RW, et al. PHENIX: a comprehensive Python-based system for macromolecular structure solution. Acta Crystallogr D Biol Crystallogr. 2010; 66:213–221. [PubMed: 20124702]

Baker NA, Sept D, Joseph S, Holst MJ, McCammon JA. Electrostatics of nanosystems: application to microtubules and the ribosome. Proc Natl Acad Sci USA. 2001; 98:10037–10041. [PubMed: 11517324]

Chen VB, Arendall WB 3rd, Headd JJ, Keedy DA, Immormino RM, Kapral GJ, Murray LW, Richardson JS, Richardson DC. MolProbity: all-atom structure validation for macromolecular crystallography. Acta Crystallogr D Biol Crystallogr. 2010; 66:12–21. [PubMed: 20057044]

Chin JY, Knowles RB, Schneider A, Drewes G, Mandelkow EM, Hyman BT. Microtubule-affinity regulating kinase (MARK) is tightly associated with neurofibrillary tangles in Alzheimer brain: a fluorescence resonance energy transfer study. J Neuropath Exp Neur. 2000; 59:966–971. [PubMed: 11089574]

de Oliveira PS, Ferraz FA, Pena DA, Pramio DT, Morais FA, Schechtman D. Revisiting protein kinase-substrate interactions: Toward therapeutic development. Sci Signal. 2016; 9:re3. [PubMed: 27016527]

Dogliotti G, Kullmann L, Dhumale P, Thiele C, Panichkina O, Mendl G, Houben R, Haferkamp S, Puschel AW, Krahn MP. Membrane-binding and activation of LKB1 by phosphatidic acid is essential for development and tumour suppression. Nat Commun. 2017; 8:15747. [PubMed: 28649994]

Emptage RP, Lemmon MA, Ferguson KM. Molecular determinants of KA1 domain-mediated autoinhibition and phospholipid activation of MARK1 kinase. Biochem J. 2017a; 474:385–398. [PubMed: 27879374]

Emptage RP, Schoenberger MJ, Ferguson KM, Marmorstein R. Intramolecular autoinhibition of checkpoint kinase 1 is mediated by conserved basic motifs of the C-terminal kinase-associated 1 domain. The J Biol Chem. 2017b; 292:19024–19033. [PubMed: 28972186]

Emsley P, Lohkamp B, Scott WG, Cowtan K. Features and development of Coot. Acta Crystallogr D Biol Crystallogr. 2010; 66:486–501. [PubMed: 20383002]

Goodwin JM, Svensson RU, Lou HJ, Winslow MM, Turk BE, Shaw RJ. An AMPK-Independent Signaling Pathway Downstream of the LKB1 Tumor Suppressor Controls Snail1 and Metastatic Potential. Mol Cell. 2014; 55:436–450. [PubMed: 25042806]

Hemsley A, Arnheim N, Toney MD, Cortopassi G, Galas DJ. A simple method for site-directed mutagenesis using the polymerase chain reaction. Nucleic Acids Res. 1989; 17:6545–6551. [PubMed: 2674899]

Krissinel E, Henrick K. Inference of macromolecular assemblies from crystalline state. J Mol Biol. 2007; 372:774–797. [PubMed: 17681537]

Lizcano JM, Goransson O, Toth R, Deak M, Morrice NA, Boudeau J, Hawley SA, Udd L, Makela TP, Hardie DG, et al. LKB1 is a master kinase that activates 13 kinases of the AMPK subfamily, including MARK/PAR-1. EMBO J. 2004; 23:833–843. [PubMed: 14976552]

Manic G, Obrist F, Sistigu A, Vitale I. Trial Watch: Targeting ATM-CHK2 and ATR-CHK1 pathways for anticancer therapy. Mol Cell Oncol. 2015; 2:e1012976. [PubMed: 27308506]

Manning G, Whyte DB, Martinez R, Hunter T, Sudarsanam S. The protein kinase complement of the human genome. Science. 2002; 298:1912–1934. [PubMed: 12471243]

Marx A, Nugoor C, Muller J, Panneerselvam S, Timm T, Bilang M, Mylonas E, Svergun DI, Mandelkow EM, Mandelkow E. Structural variations in the catalytic and ubiquitin-associated domains of microtubule-associated protein/microtubule affinity regulating kinase (MARK) 1 and MARK2. J Biol Chem. 2006; 281:27586–27599. [PubMed: 16803889]

Marx A, Nugoor C, Panneerselvam S, Mandelkow E. Structure and function of polarity-inducing kinase family MARK/Par-1 within the branch of AMPK/Snf1-related kinases. FASEB J. 2010; 24:1637–1648. [PubMed: 20071654]

Miller CJ, Turk BE. Homing in: Mechanisms of Substrate Targeting by Protein Kinases. Trends in biochemical sciences. 2018; 43:380–394. [PubMed: 29544874]

Monteverde T, Muthalagu N, Port J, Murphy DJ. Evidence of cancer-promoting roles for AMPK and related kinases. FEBS J. 2015; 282:4658–4671. [PubMed: 26426570]

Moravcevic K, Mendrola JM, Schmitz KR, Wang YH, Slochower D, Janmey PA, Lemmon MA. Kinase associated-1 domains drive MARK/PAR1 kinases to membrane targets by binding acidic phospholipids. Cell. 2010; 143:966–977. [PubMed: 21145462]

Nesic D, Miller MC, Quinkert ZT, Stein M, Chait BT, Stebbins CE. Helicobacter pylori CagA inhibits PAR1-MARK family kinases by mimicking host substrates. Nat Struct Mol Biol. 2010; 17:130–132. [PubMed: 19966800]

Otwinowski Z, Minor W. Processing of X-ray diffraction data collected in oscillation mode. Methods Enzymol. 1997; 276:307–326.

Pawson T, Kofler M. Kinome signaling through regulated protein-protein interactions in normal and cancer cells. Curr Opin Cell Biol. 2009; 21:147–153. [PubMed: 19299117]

Robert X, Gouet P. Deciphering key features in protein structures with the new ENDscript server. Nucleic Acids Res. 2014; 42:W320–324. [PubMed: 24753421]

Smits VA, Gillespie DA. DNA damage control: regulation and functions of checkpoint kinase 1. FEBS J. 2015; 282:3681–3692. [PubMed: 26216057]

Tochio N, Koshiba S, Kobayashi N, Inoue M, Yabuki T, Aoki M, Seki E, Matsuda T, Tomo Y, Motoda Y, et al. Solution structure of the kinase-associated domain 1 of mouse microtubule-associated protein/microtubule affinity-regulating kinase 3. Protein Sci. 2006; 15:2534–2543. [PubMed: 17075132]

Wu JX, Cheng YS, Wang J, Chen L, Ding M, Wu JW. Structural insight into the mechanism of synergistic autoinhibition of SAD kinases. Nat Commun. 2015; 6:8953. [PubMed: 26626945]

Yang Z, Xue B, Umitsu M, Ikura M, Muthuswamy SK, Neel BG. The signaling adaptor GAB1 regulates cell polarity by acting as a PAR protein scaffold. Mol Cell. 2012; 47:469–483. [PubMed: 22883624]

Highlights

- Crystal structure of MARK1 catalytic domain bound to its autoinhibitory KA1 domain
- The KA1 domain binds at the αD-helix between N- and C-lobes
- Kinetic studies of point mutants confirm binding interface
- KA1 domain may block peptide substrate binding site

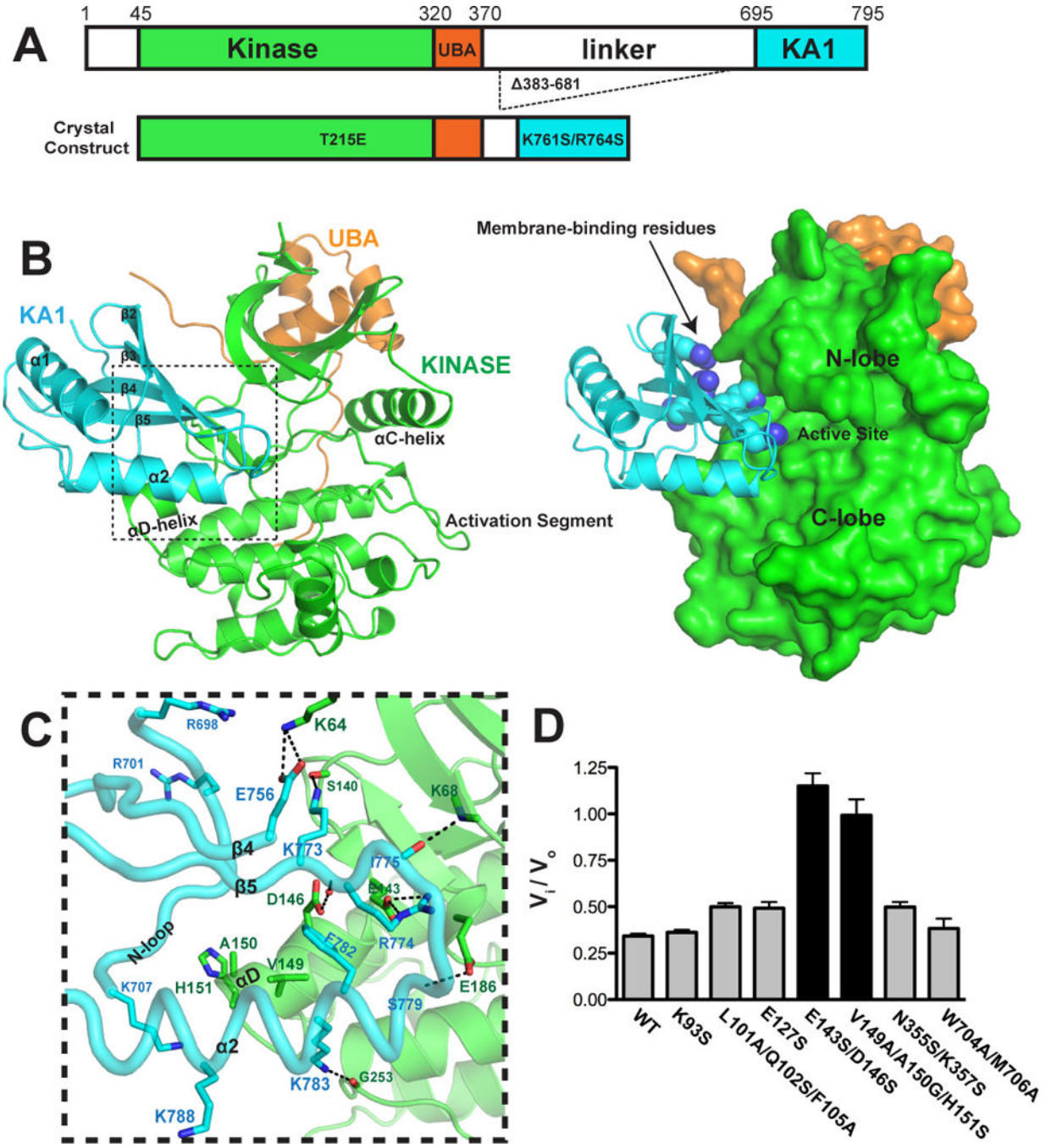

Figure 1. Crystal structure and kinase/KA1 interface validation for autoinhibited MARK1

(A) MARK1 is comprised of an N-terminal protein kinase domain (*green*), UBA domain (*orange*), linker region, and C-terminal KA1 domain (*cyan*). The crystal construct begins at residue 45 and contains a linker region deletion as well as T215E, K761S, and R764S mutations. (B) Chain A of the crystal structure of autoinhibited MARK1. The cartoon (*left panel*) is colored as in (A) with points of interest and KA1 secondary structure labeled. Surface representation (*right panel*) of the kinase/UBA domain with N-lobe, C-lobe, and active sites labeled for reference. Side chains of KA1 residues R698, R701, R771, K773,

and R774, previously implicated in membrane binding (Moravcevic et al., 2010), are displayed as spheres. (C) Close-up view of the intramolecular (biologically relevant) KA1 interface, with residues involved in the kinase/UBA – KA1 interaction shown as sticks and hydrogen bonds as dashes. KA1 domain main chain is displayed as a tube with portions of the N-loop, α1, β2, β3, and β4 removed for clarity. Water shown as a *red* sphere. Side chain labels are colored according to their domain assignment. (D) 5 μM MARK1 WT kinase/UBA construct along with surface point mutants were assayed with or without 200 μM KA1 domain and normalized to the uninhibited control. For the right-most bar, WT kinase/UBA was assayed with the W704A/M706A KA1 mutant construct. Bars colored for ability (*gray*) or inability (*black*) to inhibit the kinase/UBA domain. Error bars represent average ± standard deviation of three replicates.

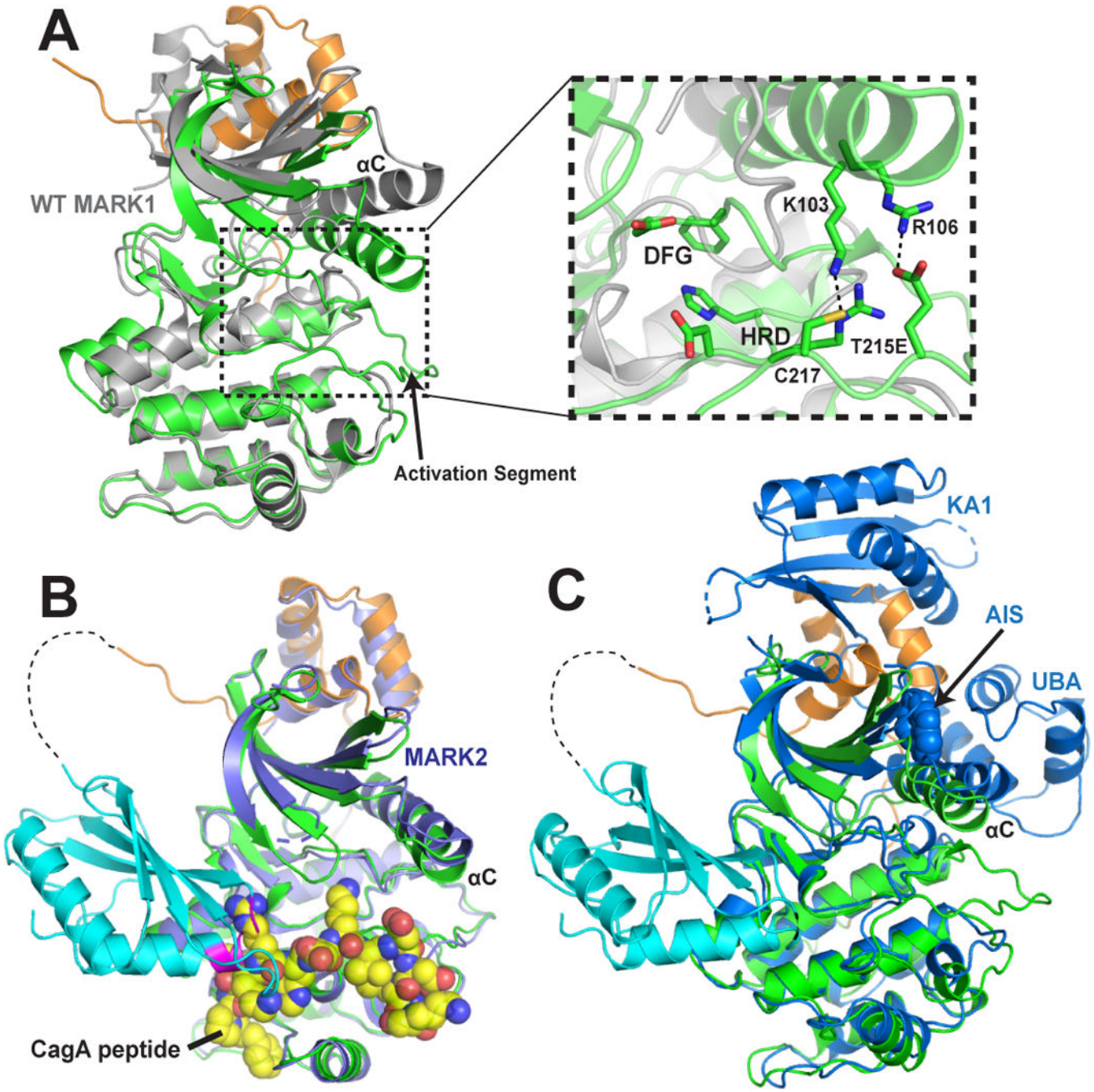

Figure 2. Structural basis for autoinhibition by the MARK1 KA1 domain

(A) Structural alignment of MARK1 kinase/UBA Chain A (colored as in Fig. 1) with WT MARK1 (*gray*) (PDB: 2HAK) shows the phosphomimetic T215E mutant adopting an active conformation. The inset shows a close-up view of the activation segment along with DFG and HRD motifs (marked). (B) Structural alignment of mini-MARK1 (including KA1 domain in cyan) with MARK2 (*purple*) bound to an *H. pylori* inhibitory peptide (*yellow* spheres) (PDB: 3IEC), showing overlap between binding sites on the kinase for the KA1 domain and *H. pylori* inhibitory peptide. The dotted line represents residues in mini-

MARK1 that could not be modeled due to lack of electron density. Residues G777-A781 of the KA1 domain (*magenta*) occupy the same space on the C-lobe as peptide in the alignment. (C) Structural alignment of mini-MARK1 (chain A) with SAD-A (*blue*) (PDB: 4YOM), revealing a unique binding mode for the MARK1 KA1 domain (cyan) on the opposite side of the N-lobe from that seen for the SAD-A KA1 domain (blue). Hydrophobic side chains from the AIS (W522, F523) that are crucial for SAD-A autoinhibition, are shown as *spheres*, and pointed out with a black arrow.

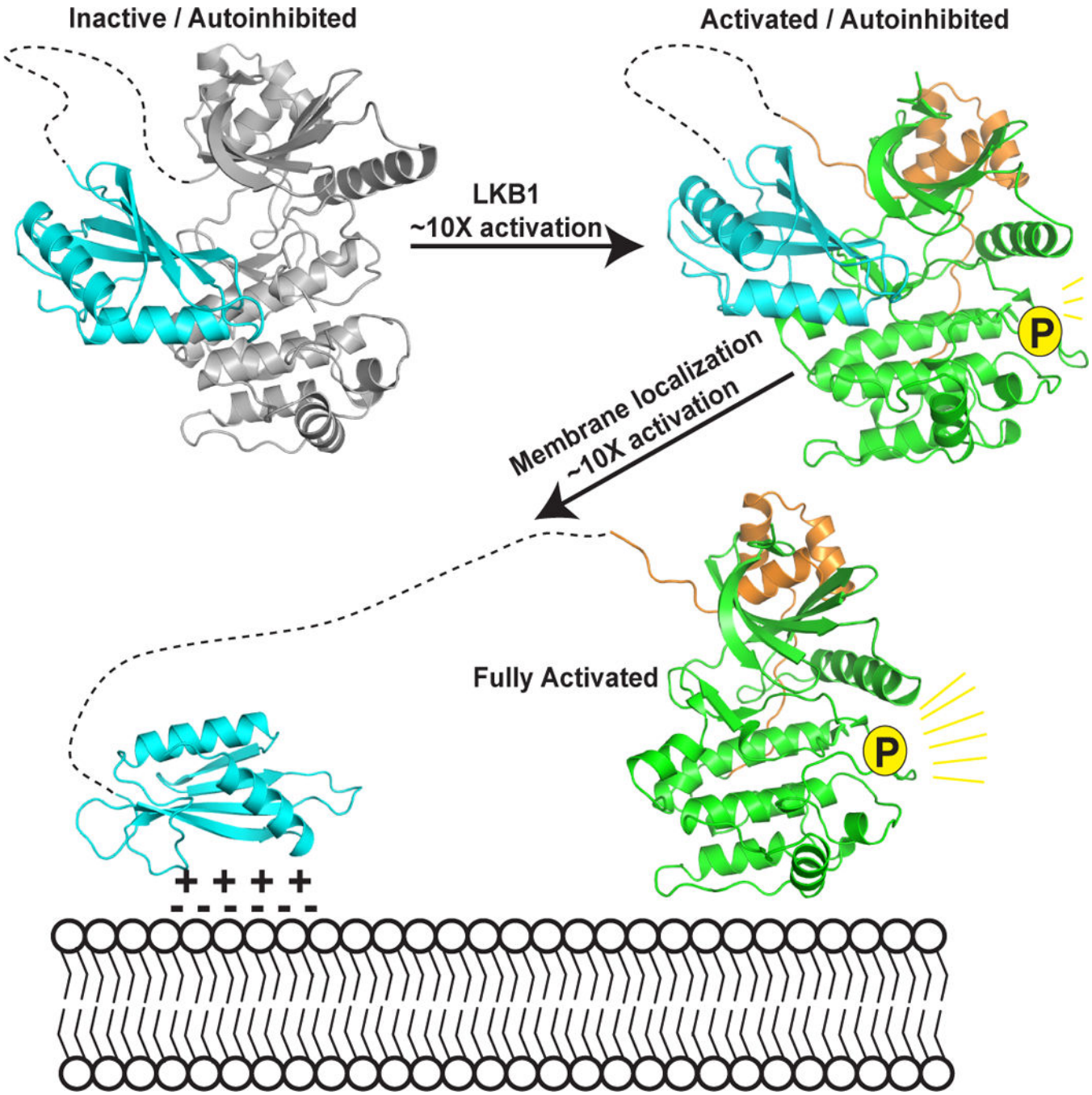

Figure 3. Proposed multi-step mechanism for MARK1 activation

This model depicts the proposed full activation mechanism for MARK1, which includes activation segment phosphorylation and disengagement of KA1-mediated autoinhibition by localization to anionic membranes. The crystal structure reported here represents the "activated/autoinhibited" form of MARK1, colored as in Fig. 1. The "inactive/autoinhibited" form is modeled using the structural alignment (Fig. 2A) with WT MARK1 kinase/UBA crystal structure (PDB: 2HAK) shown in *grey*.

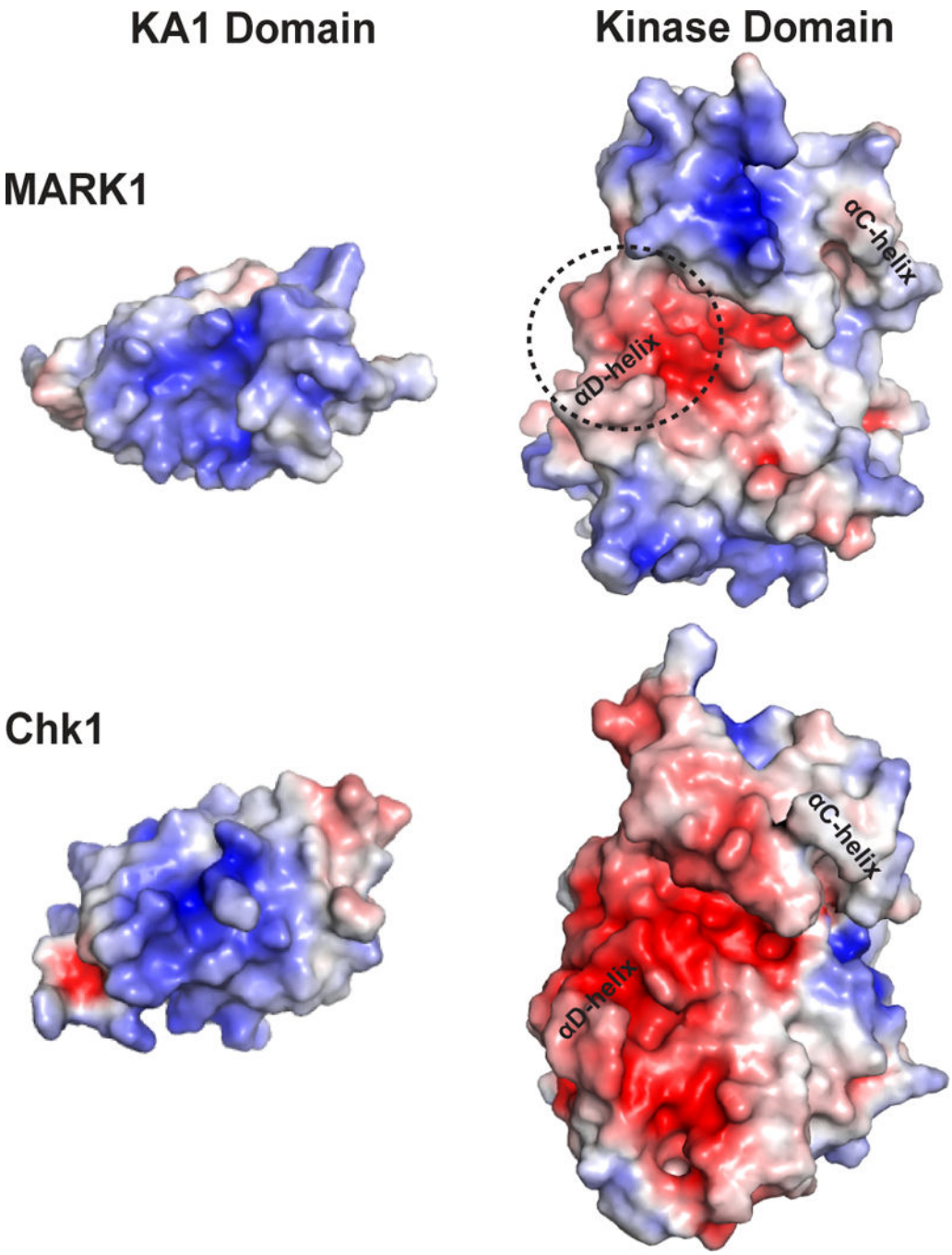

Figure 4. Surface charge properties of kinase/KA1 domains at the αD-helix interface

Electrostatic surface potentials were calculated for the KA1 and kinase domains of MARK1 (this work) or Chk1 (PDB: 5WI2 and 1IA8) using the Adaptive Poisson-Boltzmann Solver (Baker et al., 2001), scaled from −5.0 (*red*) to +5.0 (*blue*) kT/e. For the MARK1 KA1 domain, the kinase-interacting region is facing the reader, whereas the KA1-interacting region of the kinase domain is indicated with the *dashed* circle. αD-helix and αC-helix

locations on the generated surface are indicated. Chk1 surfaces are displayed in orientations analogous to those used for MARK1.

TABLE 1

Data collection statistics

Space group	C 1 2 1
Unit cell [a,b,c (Å) α,β,γ (°)]	170.0, 69.6, 104.0 90, 124.3, 90
Wavelength (Å)	1.0
Resolution (Å)	50.0-2.5 (2.54-2.50)
R_{merge}	0.064 (0.317)
I/σ	36.1 (2.1)
Completeness (%)	98.9 (94.5)
Redundancy	3.3 (2.7)
No. of unique reflections	34,570
REFINEMENT	
R_{work}/R_{free}(%)	20.2/25.2
No. of atoms [average *B* factor (Å^2)]	
Protein	6,634 (77.9)
Water	68 (67.5)
Ramachandran plot (%)	
Favored	96.0
Allowed	4.0
RMSD	
Bond length (Å)	0.01
Bond anges (deg)	1.29

*Values in parenthesis indicate highest-resolution shell